COMMUNICATIONS IN NUMERICAL METHODS IN ENGINEERING, Vol. 10, 683–697 (1994)

CONVERGENCE OF STRESS MAXIMA IN FINITE ELEMENT COMPUTATIONS

ZOHAR YOSIBASH AND BARNA A. SZABÓ
Center for Computational Mechanics, Washington University, Campus Box 1129, St. Louis, MO 63130, U.S.A.

SUMMARY

The convergence of stress maxima, computed directly from finite element solutions, is investigated with respect to a family of exact solutions characterized by varying degrees of smoothness. The performances of h- and p-extensions and the product and trunk spaces are evaluated and documented with respect to a family of benchmark problems. In uniform p-extensions a characteristic pattern in the convergence of stress maxima was observed. There does not appear to be a clear-cut advantage of the product space over the trunk space in this respect. The much faster convergence of stress maxima in the case of p-extensions, as compared with h-extensions, is evident from the results.

INTRODUCTION

The problem of quality control in finite element computations has been the subject of many investigations. Most of the available work has been concerned with estimation and control of error in energy norm. It is known that for reasonable Poisson ratios the energy norm measure of the error is closely related to the root-mean-square measure of error in stresses. These are average measures, however. In most cases engineers are interested in determining the location and magnitude of the largest principal stress, or, equivalently, the stress concentration factor. Typically, this is done by direct computations. Therefore the accuracy of stress data computed by direct methods is of considerable practical interest.

Indirect computation of stresses have been shown to be superior to direct methods (see, for example, References 1–3). Computer implementation of indirect methods is difficult, however, because different procedures are required at and near boundaries from the interior. In searching for stress maxima, the stress values are computed in many points, which makes it necessary to perform computations efficiently. None of the generally available finite element programs offer superconvergent extraction procedures for stresses at present.

In this paper the convergence of the largest stress computed directly from the finite element solution, that is, by differentiating the displacement function to obtain the strain components, then using the stress–strain law for computing the stresses, is examined with reference to a family of model problems. The model problems are constructed in such a way that the corresponding exact solutions are known and the smoothness of the exact solutions can be varied by changing one parameter. The construction of model problems and the results of numerical studies are presented in the following.

CCC 0748–8025/94/090683–15

Received 5 September 1993
Revised 17 February 1994

THE MODEL PROBLEMS

Consider an infinite plate containing an elliptic hole of major axis a and minor axis b. The plate is loaded in its plane by uniform tension at infinity. Firstly, the exact solution is obtained by classical methods. A subdomain containing the elliptic hole is then selected and the tractions corresponding to the exact solution are imposed on the boundaries of the subdomain. In this way a family of problems is defined. The smoothness of the solutions depends on the ratio b/a.

The exact solutions are constructed using the complex representation of the Airy stress functions (see Reference 4). It is known that every Airy stress function can be represented in terms of two analytic complex functions $\phi(z)$ and $\psi(z)$ in the domain describing the body. The stress components can be related to $\phi(z)$ and $\psi(z)$ as shown in the following.

If $\phi(z)$ and $\psi(z)$ are the solution to a 2-D problem in a domain $\Omega(z)$, we may transform $\Omega(z) \leftarrow \Omega'(\zeta)$ ($\zeta = \rho e^{i\theta}$, $z = re^{it}$) using conformal mapping. By this method it is possible to obtain solutions on a variety of domains, provided that the mapping $z = \omega(\zeta)$ is known and conformal, and the solution in $\Omega'(\zeta)$ is known. In the following a circular hole in an infinite plate is used as the geometry in $\Omega'(\zeta)$, for which a well known solution exists, and this domain is transformed to $\Omega(z)$ such that an ellipse in an infinite plate is obtained. Defining $\Phi(z) = \phi'(z)$, and $\Psi(z) = \psi'(z)$, we obtain:

$$\tau_{\rho\rho} + \tau_{\theta\theta} = 4\Re\Phi(\zeta) \tag{1}$$

$$(\tau_{\theta\theta} - \tau_{\rho\rho}) + 2i\tau_{\rho\theta} = \frac{2\zeta^2}{\rho^2\overline{\omega'(\zeta)}}\{\overline{\omega(\zeta)}\Phi'(\zeta) + \omega'(\zeta)\Psi(\zeta)\} \tag{2}$$

The maximum stress at the edge of an elliptic hole in an infinite plate, loaded by tension at infinity, is a function of the ratio b/a only. For the case $b/a = 1$, the ellipse is a circle and the stress concentration factor is known to be 3. For the case $b/a \to 0$, the ellipse becomes a crack and the stress concentration becomes infinity.

The transformation of a circular hole of radius R in an infinite plate into an elliptic hole in an infinite plate, located at the origin, with major axis ($a = R(1 + m)$) and minor axis ($b = R(1 - m)$) is given by

$$z = \omega(\zeta) = R\left(\zeta + \frac{m}{\zeta}\right) \quad (R > 0, 0 \leqslant m < 1) \tag{3}$$

By a suitable choice of R and m, one may obtain ellipses of any dimension and shape.

Let the state of stress at infinity be tension of magnitude P in a direction forming an angle α with the x-axis. For this loading (see Reference 4 p. 338):

$$\phi(\zeta) = \frac{PR}{4}\left(\zeta + \frac{2e^{i\alpha} - m}{\zeta}\right) \tag{4}$$

$$\psi(\zeta) = -\frac{PR}{2}\left[e^{-2i\alpha}\zeta + \frac{e^{2i\alpha}}{m\zeta} - \frac{(1 + m^2)(e^{2i\alpha} - m)}{m}\frac{\zeta}{\zeta^2 - m}\right] \tag{5}$$

and

$$\Phi(\zeta) = \frac{\phi'(\zeta)}{\omega'(\zeta)}, \qquad \Psi(\zeta) = \frac{\psi'(\zeta)}{\omega'(\zeta)} \tag{6}$$

A solution to this problem was found by a different method by C. E. Inglis in 1913 (see

Reference 5). For $R = 1$ the stresses corresponding to $\Phi(\zeta)$ and $\Psi(\zeta)$ are as follows:

$$\tau_{\rho\rho} + \tau_{\theta\theta} = \frac{P}{f(\rho,\theta)} \{\rho^4 - m^2 + 2m\cos(2\alpha) - 2\rho^2 \cos 2(\alpha - \theta)\}$$

$$\begin{aligned}\tau_{\theta\theta} - \tau_{\rho\rho} = \frac{P}{f^2(\rho,\theta)} \{&\cos 2(\theta - \alpha)[2\rho^6 - \rho^8 - 3m^2\rho^4 - 3\rho^4 - m^2] - 2m^2\rho^2 \cos 2(\alpha + \theta) \\ &+ m\rho^2(1 + \rho^4)\cos 2(\alpha - 2\theta) + m\rho^2(3 + \rho^4 + 2m^2)\cos 2\alpha \\ &+ (\rho^4 - m^2)[-2m\rho^2 \cos 2\theta + \rho^2(1 + m^2)]\}\end{aligned} \tag{7}$$

$$\begin{aligned}\tau_{\rho\theta} = \frac{2P}{f^2(\rho,\theta)} &\{\rho^6 \sin 2(\alpha - \theta) - m^2\rho^2 \sin 2(\alpha + \theta) + (m\rho^6 + m^3\rho^2)\sin 2\theta\} \\ -\frac{P}{f^2(\rho,\theta)} &\{\sin 2(\theta - \alpha)[\rho^8 + 2m^2\rho^4 - 3\rho^4 - m^2 - m^2\rho^4] + \sin 2\alpha[3m\rho^6 - 3m\rho^2] \\ &- 2m^2\rho^4 \sin 2(\theta + \alpha) + \sin 2(\alpha - 2\theta)[m\rho^6 - m\rho^2] \\ &+ 2m\rho^4(1 + m^2)\sin 2\theta\}\end{aligned}$$

where $f(\rho,\theta) = \rho^4 - 2m\rho^2 \cos 2\theta + m^2$.

Curves of constant ρ in the ζ-plane (which are circles of radius ρ) are mapped into ellipses with major axis $a = (\rho + m/\rho)$ and minor axis $b = (\rho - m/\rho)$. We may choose as the outer curved edge of the ellipse $\rho = \text{const.} > 1$.

The finite dimensional subdomain selected for this investigation is shown in Figure 1. It is bounded by two ellipses corresponding to $\rho = 1$ and $\rho = 4$ and the x- and y-axes. The loading is uniform tension at infinity in the direction of the y-axis (i.e. $\alpha = \pi/2$). Therefore the x- and y-axes are axes of symmetry. The inner elliptical boundary ($\rho = 1$) is stress-free. The normal traction component T_N and the tangential traction component T_T on the outer elliptical

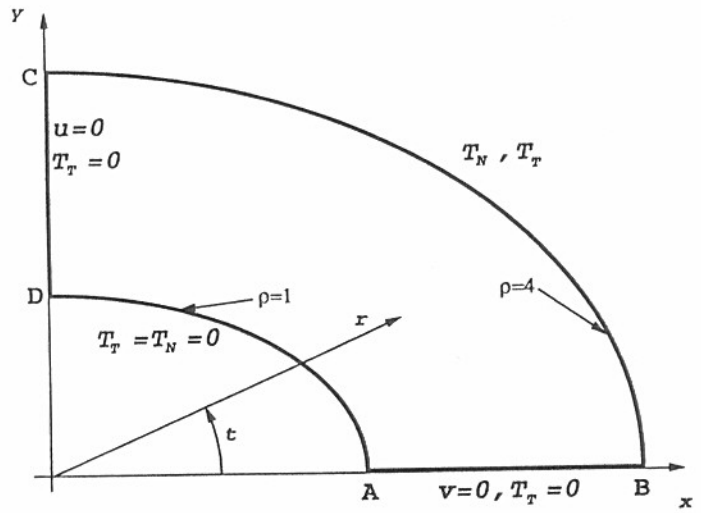

Figure 1. Solution domain and boundary conditions

boundary are:

$$T_N(r,t) = \tau_{\rho\rho}(r(\rho,\theta), t(\rho,\theta)), \qquad T_T(r,t) = \tau_{\rho\theta}(r(\rho,\theta), t(\rho,\theta))$$

where $\tau_{\rho\theta}$ and $\tau_{\rho\rho}$ are obtained from (7)

$$\begin{aligned}\tau_{\rho\theta} &= \frac{P}{2f^2(\rho,\theta)}\{\sin 2\theta[2\rho^2(\rho^2-1)(1+m)(\rho^2-m^2)+(\rho^4-1)(m^2+\rho^4)] \\ &\quad + \sin 4\theta(1-\rho^4)\rho^2 m\} \\ \tau_{\rho\rho} &= \frac{P}{2f^2(\rho,\theta)}\{(\rho^4-2m-m^2)(\rho^2-m^2)(\rho^2-1) \\ &\quad + \cos 2\theta[(\rho^4+m^2)(4\rho^2-\rho^4-1)-2\rho^4(m^2+1)]+2m\rho^2(1-\rho^2)^2 \\ &\quad \cos^2 2\theta\}\end{aligned} \tag{8}$$

Note that the mapping $z = \omega(\zeta)$ is conformal, so that, if $\tau_{\rho\rho}$ is perpendicular to $\tau_{\rho\theta}$ in the ζ-plane, then the corresponding stresses in the z-plane are also perpendicular.

The maximum stress is obtained for $\tau_{\theta\theta}$ at point A:

$$\tau_{\theta\theta}\,|_{\max} = \frac{P}{2}\frac{3-2m-m^2}{(1-m)^2} = P\left(1+\frac{2a}{b}\right) \tag{9}$$

Remark. Since the exact solution is known, it would have been possible to impose displacement rather than tractions on the boundary. This would have required, however, enforcement of the boundary conditions by restriction on the space of admissible functions. Approximation of the exact displacement functions by polynomials would have introduced an error and convergence of the potential energy with respect to increasing polynomial degrees would not have been necessarily monotonic.

Remark. In order to specify the normal and tangential tractions on the outer boundaries, we need to obtain the relationship between cylindrical co-ordinates (r,t) and (ρ,θ). On boundary BC, $\rho = \rho_1 = \text{const.}$, and therefore the needed relationship is

$$\theta\,|_{BC} = \tan^{-1}\left\{\left(\frac{\rho_1^2+m}{\rho_1^2-m}\right)\tan(t)\right\} \tag{10}$$

Computation of potential energy

The finite element method based on displacement formulation selects that displacement vector $(u_{x\mathrm{FE}}, u_{y\mathrm{FE}})$ from the finite element space which minimizes the energy norm of the error. A well developed theoretical basis exists for the estimation of error in energy norm for the h-, p- and hp-extensions (see Reference 6). In the following the error in maximal stress is correlated with the error in energy norm, which can be estimated with good accuracy from finite element solutions. However, in this case the exact solution is known, and therefore we are in a position to compute the exact potential energy. In this way the error in energy norm of the finite element solution can be computed without resorting to estimation.

The displacements in $\Omega'(\zeta)$ plane can be computed from $\phi(\zeta)$ and $\psi(\zeta)$ presented in (4) and (5) as follows (see Reference 4, p. 183):

$$u_\rho + iu_\theta = \frac{1}{2\mu\,|\,\omega'(\zeta)\,|}\frac{\bar{\zeta}}{\rho}\omega'(\zeta)\left[\varkappa\phi(\zeta) - \frac{\omega(\zeta)}{\omega'(\zeta)}\overline{\phi'(\zeta)} - \overline{\psi(\zeta)}\right] \tag{11}$$

where μ is the shar modulus, ν is Poissons' ratio and

$$\varkappa = \begin{cases} 1 - 3\nu & \text{for plane strain} \\ \dfrac{3 - \nu}{1 + \theta} & \text{for plane stress} \end{cases}$$

After some algebraic manipulations the displacements u_ρ and u_θ for $R = 1$ are found to be:

$$u_\rho = \frac{P}{8\mu\rho\sqrt{f(\rho,\theta)}} \{(\varkappa - 1)(\rho^4 + 2m + m^2) + 2\rho^2(m+1)^2 + 2[1 - \rho^4 - \rho^2(1+\varkappa)(1+m)]\cos 2\theta\}$$

$$u_\theta = -\frac{P}{4\mu\rho\sqrt{f(\rho,\theta)}} [\rho^2(1-\varkappa) - \rho^4 - 1]\sin 2\theta \tag{12}$$

For a solution domain loaded by tractions only without body forces the potential energy Π is

$$\Pi = -\oint (T_N u_N + T_T u_T)\, ds \tag{13}$$

where the contour integral is over the boundary of the solution domain and (T_N, T_T), (u_N, u_T) are the tractions and displacements in the normal–tangential reference frame with respect to the boundaries. On the solution domain presented in Figure 1, (13) is simplified to

$$\Pi = -\int_B^C (T_N(r,t)u_N(r,t) + T_T(r,t)u_T(r,t))\, ds \tag{14}$$

For the ellipse BC, ds can be shown to be

$$ds = b \frac{\left[1 - \left(1 - \dfrac{b^4}{a^4}\right)\cos^2 t\right]^{1/2}}{\left[1 - \left(1 - \dfrac{b^2}{a^2}\right)\cos^2 t\right]^{3/2}} dt \qquad 0 \leqslant t \leqslant \pi/2 \tag{15}$$

The mapping $z = \omega(\zeta)$ is conformal, which guarantees that in the ζ-plane $T_N \perp T_T \to \tau_{\rho\rho} \perp \tau_{\rho\theta}$ and $u_N \perp u_T \to u_\rho \perp u_\theta$. BC is the portion of a circle with radius $\rho = \text{const.}$, and $0 \leqslant \theta \leqslant \pi/2$. Using (10) we have the relationships:

$$\cos^2 t = \frac{(\rho^2 + m)^2 \cos^2\theta}{(\rho^2 - m)^2 + 4m\rho^2\cos^2\theta} \tag{16}$$

$$dt = \frac{(\rho^2 - m)(\rho^2 + m)}{(\rho^2 - m)^2 + 4m\rho^2\cos^2\theta} d\theta \tag{17}$$

and substituting into (15), ds becomes

$$ds = \frac{\sqrt{f(\rho,\theta)}}{\rho} d\theta \tag{18}$$

Substituting (8), (12) and (18) into (14) one obtains

$$\Pi = \frac{-P^2}{16\mu\rho^2} \int_0^{\pi/2} \frac{1}{f^2(\rho,\theta)} \{(A_2 + A_3\cos 2\theta)(B_3 + B_4\cos 2\theta + B_5\cos^2 2\theta) - 2A_1\sin^2 2\theta(B_1 + 2B_2\cos 2\theta)\}\, d\theta \tag{19}$$

where

$$
\begin{aligned}
A_1 &= \rho^2(1-\varkappa) - \rho^4 - 1 \\
A_2 &= (\varkappa - 1)(\rho^4 + 2m + m^2) + 2\rho^2(m+1)^2 \\
A_3 &= 2[1 - \rho^4 - \rho^2(1+\varkappa)(1+m)] \\
B_1 &= 2\rho^2(\rho^2 - 1)(1+m)(\rho^2 - m^2) + (\rho^4 - 1)(\rho^4 + m^2) \\
B_2 &= (1-\rho^4)\rho^2 m \\
B_3 &= (\rho^4 - 2m - m^2)(\rho^2 - m^2)(\rho^2 - 1) \\
B_4 &= (\rho^4 + m^2)(4\rho^2 - \rho^4 - 1) - 2\rho^2(m^2+1) \\
B_5 &= 2m\rho^2(1-\rho^2)^2
\end{aligned}
\tag{20}
$$

and $\rho = \text{const.} = 4$.

For an isotropic material under the assumption of plane stress, Young's modulus $1{\cdot}0$ and Poisson's ratio $0{\cdot}3$, the following values for different ms are obtained:

$$
\begin{aligned}
\Pi_{EX}(m = 0) &= -16{\cdot}33892955, & \Pi_{EX}(m = 0{\cdot}25) &= -26{\cdot}70957359 \\
\Pi_{EX}(m = 0{\cdot}05) &= -27{\cdot}08611104, & \Pi_{EX}(m = 0{\cdot}75) &= -27{\cdot}45638123 \\
\Pi_{EX}(m = 0{\cdot}85) &= -27{\cdot}59927711, & \Pi_{EX}(m = 0{\cdot}9) &= -27{\cdot}66902911
\end{aligned}
$$

The exact error in energy norm can now be computed from

$$
(\| e \|_E)_{EX} = \sqrt{\left| \frac{\Pi_{EX} - \Pi_{FE}}{\Pi_{EX}} \right|} \tag{21}
$$

NUMERICAL EXPERIMENTS

Numerical experiments were performed with the objective to evaluate the convergence characteristics of various extension procedures. The computer code PEGASYS[a] was used for this purpose. PEGASYS has h- and p-extension capabilities and allows the choices of product and trunk spaces for quadrilateral elements. By definition, the trunk space of degree p spans the set of monomials $\xi^i\eta^j$, $i + j \leqslant p$ augmented by the monomial $\xi\eta$ for $p = 1$ and by the monomials $\xi^p\eta$, $\xi\eta^p$ for $p \geqslant 2$ on the standard quadrilateral element defined by $\Omega_{st}^{(q)} = \{\xi, \eta \mid |\xi| \leqslant 1, |\eta| \leqslant 1\}$. The product space spans the set of monomials $\xi^i\eta^j$, $i, j = 0, 1, 2, \ldots, p$ on $\Omega_{st}^{(q)}$. Elements are mapped by the blending function method. Therefore the boundaries are represented exactly in the stiffness matrix and load vector computations. The load vectors were computed by evaluating the applied tractions in 14 Gauss points along the loaded edge of each element and integrated numerically, using double precision operations. Isotropic material and Poisson's ratio of $0{\cdot}3$ was used, under the assumption of plane stress.

The direct method of extraction procedure is described in detail in Reference 7, Section 11.4.1. The strains were computed from the displacement components and the stresses from the appropriate stress–strain relationship. The trial functions over each element are polynomials of degree $1 \leqslant p \leqslant 8$, and the integration scheme uses $(p+3)(p+3)$ Gauss integration points over each quadrilateral.

The potential energy corresponding to the finite element solution (Π_{FE}) for a domain loaded by tractions only is computed from the product of the load vector and the solution vector.

---

[a] Engineering Software Research and Development, Inc., 7750 Clayton Road, Suite 204, St. Louis, MO 63117.

The point-wise stresses extracted by direct computations from the finite element solution do not in general converge monotonically even though the error in energy norm does, and their rate of convergence is dependent on the smoothness of the exact solution.

By varying m from 0 to 0·9, we can obtain stress concentration factors[b] at point A (see Figure 1), which range from 3 (corresponding to the circular hole in the infinite plate) to 39, respectively.

The first step in this study was to ensure that PEGASYS handles the complicated expressions for the normal and tangential tractions properly and the errors introduced by numerical integration are small. To verify this, the circular hole in an infinite plate problem was tested ($m = 0$). The stress at infinity was taken to be $P = 2$. Using the trunk space, the solution converged to 0·05 per cent error in energy norm and to 0·03 per cent error in the stress at point A at $p = 8$. This indicates that no significant errors were induced by numerical integration.

As the parameter m is increased, ellipses are obtained which have increasing stress concentration factors at point A. The four levels of mesh refinement used in conjunction with p-extensions are presented in Figure 2. These meshes are referred to as 'regular meshes', in contrast with 'graded meshes' introduced in the following. (At $p = 8$ and the trunk space, for the 6-element mesh there are 408 degrees of freedom (DOF), for the 9-element mesh 588 DOF, for the 12-element mesh 768 DOF, and for the 15-element mesh 948 DOF).

We have observed that the errors both in the strain energy and in the calculated stresses were comparatively high for the models for which $m \geqslant 0{\cdot}75$. Therefore the domains were remeshed using meshes which are graded in a geometric progression in the vicinity of point A with the factor 0·17. This is the optimal grading for p-extension in the vicinity of singular points.[7] Summaries of the results are presented in Tables I–III. Tables I and II present the results obtained using the regular and graded meshes, respectively, while in Table III the comparison

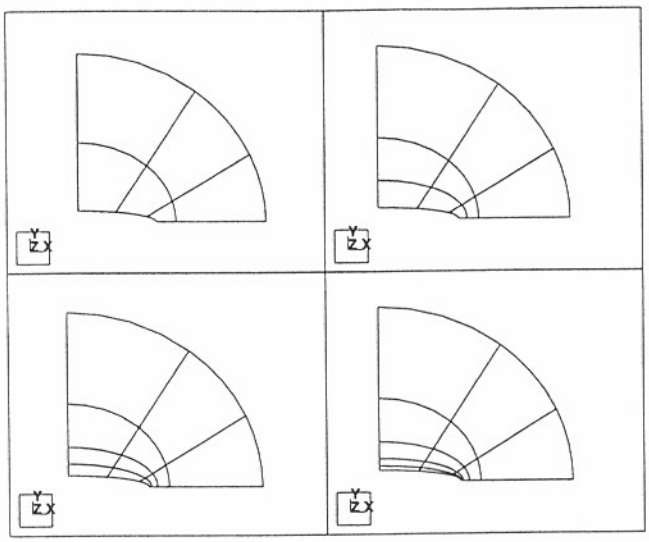

Figure 2. Finite element meshes with four levels of refinement

[b] The stress concentration factor is defined as the ratio $\tau_{\theta\theta}(A)/P$.

between them is summarized. In Tables I–III the estimated error in energy norm is defined by $\| e \|_E$, and the estimated asymptotic rate of convergence in energy norm by β. The error estimates are obtained by extrapolation. For detailed discussion on the estimation of $\| e \|_E$ and β we refer to Chapter 4 in Reference 7.

We plotted the stress as a function of number of degrees of freedom to better understand their convergence behaviour. A typical convergence plot for the case when $m = 0{\cdot}75$, using both the product space and the trunk space and for a regular mesh with 12 elements, is presented in Figure 3. This plot shows the typical behaviour of the stresses which we have observed in almost all cases, namely, the stresses tend to 'overshoot' the exact value and they

Table I. Trunk space – regular mesh

DOF	m	a	b	$\| e \|^*_E$(%)	β^*	$\tau^{EX}_{\theta\theta}$	$\tau^{FE*}_{\theta\theta}$	$e_\tau = \frac{\tau^{FE}_{\theta\theta} - \tau^{EX}_{\theta\theta}}{\tau^{EX}_{\theta\theta}}$ (%)
408	0	1	1	0·05	3·61	6·0	6·0018	0·03
408	0·25	1·25	0·75	0·12	2·73	8·666	8·6744	0·09
408	0·5	1·5	0·5	0·8	1·78	14	14·1849	1·32
588				0·13	2·36		14·1174	0·83
408	0·75	1·75	0·25	3·24	0·78	30	29·4923	−1·69
588				1·01	1·55		30·6617	2·20
768				0·28	1·90		30·8285	2·76
588	0·85	1·85	0·15	4·06	0·52	51·333	47·9188	−6·65
768				1·13	1·18		51·6373	0·59
588	0·90	1·9	0·1	5·75	0·44	78	64·0595	−17·8
768				2·15	0·81		71·0440	−8·92

Table II. Trunk space – graded mesh

DOF	m	a	b	$\| e \|^*_E$(%)	β^*	$\tau^{EX}_{\theta\theta}$	$\tau^{FE*}_{\theta\theta}$	$\frac{\tau^{FE}_{\theta\theta} - \tau^{EX}_{\theta\theta}}{\tau^{EX}_{\theta\theta}}$ (%)
408	0·75	1·75	0·25	2·73	0·86	30	29·733	−0·89
588				0·33	2·05		30·819	2·73
768				0·19	2·45		30·256	0·85
588	0·85	1·85	0·15	1·32	1·19	51·333	51·423	0·17
768				0·79	1·44		52·734	2·72

Table III. Regular against graded mesh, trunk space

DOF	m	$\| e \|^{(R)*}_E$(%)	$\| e \|^{(G)*}_E$(%)	$\beta^{(R)*}$	$\beta^{(G)*}$	$e_\tau{}^{(R)*}$(%)	$e_\tau{}^{(G)*}$(%)
408	0·75	3·24	2·73	0·78	0·86	−1·69	−0·89
588		1·01	0·33	1·55	2·05	2·20	2·73
768		0·28	0·19	1·90	2·45	2·76	0·85
588	0·85	4·06	1·32	0·52	1·19	−6·65	0·17
768		1·13	0·79	1·18	1·44	0·59	2·72

* At $p = 8$

converge to the exact value at a rate which depends on the smoothness. We observed a monotonic convergence of the stress to the exact value only for one case ($m = 0{\cdot}75$, six elements). The confidence in the results is much higher when monotonic convergence occurs, provided that the convergence curve approaches the zero slope. However, from experience gained so far this monotonic convergence of the maximal stress is rare. The 'knee' at $p = 2, 3$, clearly visible, was observed in many cases.

The 'overshoot' may be large for smooth solutions (when $m = 0$, for example), but the convergence thereafter is fast. As $m \to 1$ the exact solution becomes less and less smooth, and the convergence after the 'overshoot' occurs slowly. Simply observing the convergence curve one may erroneously think that 'The curve is almost flat, so convergence was probably achieved'. Figure 3 illustrates this phenomenon for $m = 0{\cdot}75$.

In Figure 3 the case 'combined trunk and product space' represents a discretization where product space is used on the element at the tip of the ellipse, and trunk space is used for all other elements. The results show that at the higher p-levels ($p = 6,7,8$) the error is virtually the same as if the product space had been used on all elements. This indicates that (a) the product space generally yields better results than the trunk space for the same p-levels and (b) the error in the maximal stress can be reduced by local refinement.

In Figure 4 we show the absolute value of the relative error in maximum stress as compared to the relative error in energy norm on a log–log scale for $m = 0{\cdot}85$. In Figure 5 the same information is shown for $m = 0{\cdot}75$, where the maximum stress converges monotonically. When the solution is smooth, and Poisson's ratio is not close to 1/2, then the maximal stress converges at about the same rate as the finite element solution in energy norm. However, when the solution is not smooth, and the convergence in the maximal stress is not monotonic, then there is no close correlation between the error in energy norm and the error in maximal stress. In Figure 4, for example, at low p-levels the error decreases and then increases due to the

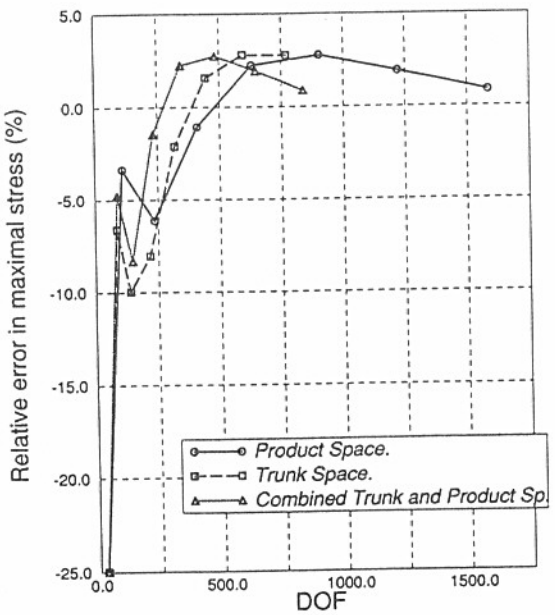

Figure 3. p-convergence curve for $m = 0{\cdot}75$, 12 elements, regular mesh

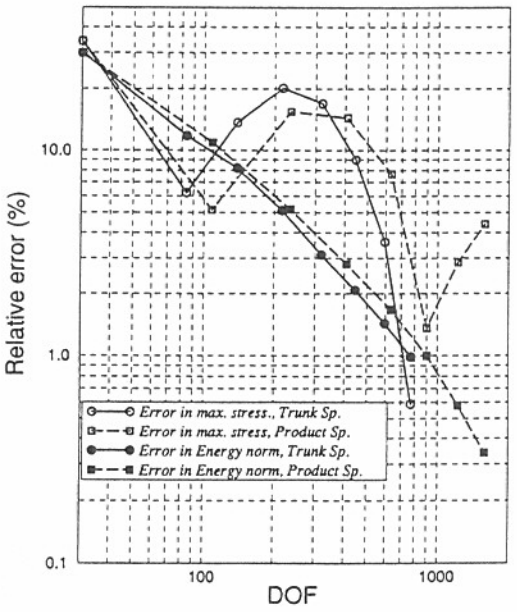

Figure 4. p-convergence curve for $m = 0{\cdot}85$, 12 elements, regular mesh, log–log scale

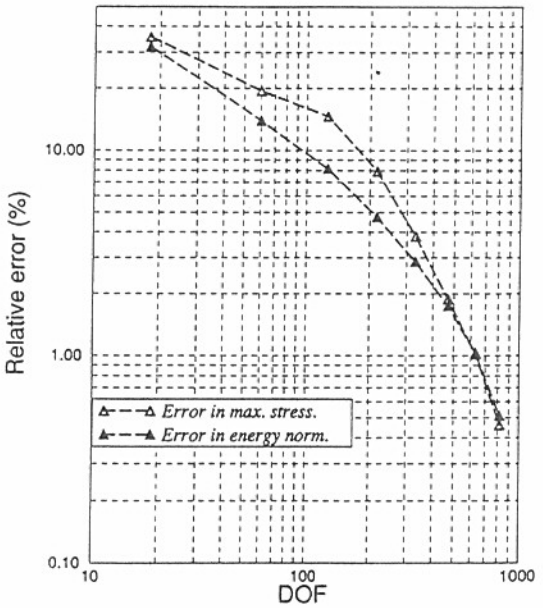

Figure 5. p-convergence curve for $m = 0{\cdot}75$, 6 elements, product space, regular mesh, log–log scale

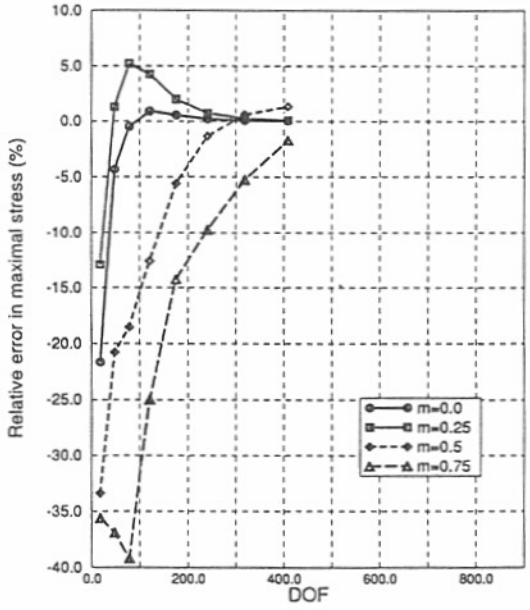

Figure 6. Convergence curves for the regular 6-element mesh and trunk space for various m values

'knee', thereafter the error decreases as the maximal stress approaches the exact value from below, but then the maximal stress overshoots the exact value so the error increases again.

The behaviour of the point-wise stress as the exact solution becomes less and less smooth (m increases) is best illustrated by Figure 6, where we show the convergence of the stress using the trunk space over the regular 6-element mesh for $m = 0, 0{\cdot}25, 0{\cdot}5, 0{\cdot}75$. The deterioration of the stress accuracy as m increases, and the 'overshoot' phenomenon, are clearly visible. For $m = 0{\cdot}75$, the curve tends to 'overshoot' the exact value, but at $\rho = 8$ the stress is still below the exact value. The same behaviour was visible when using the product space as well.

The influence of various meshes while using p-extension is shown in Figure 7, where we compare the stress convergence for the case $m = 0{\cdot}75$, using the trunk space over meshes shown in Figure 2. The pattern of convergence is similar for the three mesh refinements.

Meshes graded in geometric progression with the common factor of $0{\cdot}17$ in the vicinity of the stress concentration improve the convergence of the stress, but the pattern of convergence of the stresses as p increases remain the same as for regular meshes.

Comparison between product space and trunk space

The question of whether the product space has any advantage over the trunk space (using the p-extension over a fixed mesh), when stress maxima are of interest was investigated. The number of degrees of freedom was used as the basis of comparison. This comparison tends to favour the trunk space because for a fixed number of degrees of freedom the front size associated with the product space is smaller than the front size associated with the trunk space.

The dependence of the accuracy on the space chosen appears to be completely random, meaning that for a fixed number of degrees of freedom in some cases the stress is more

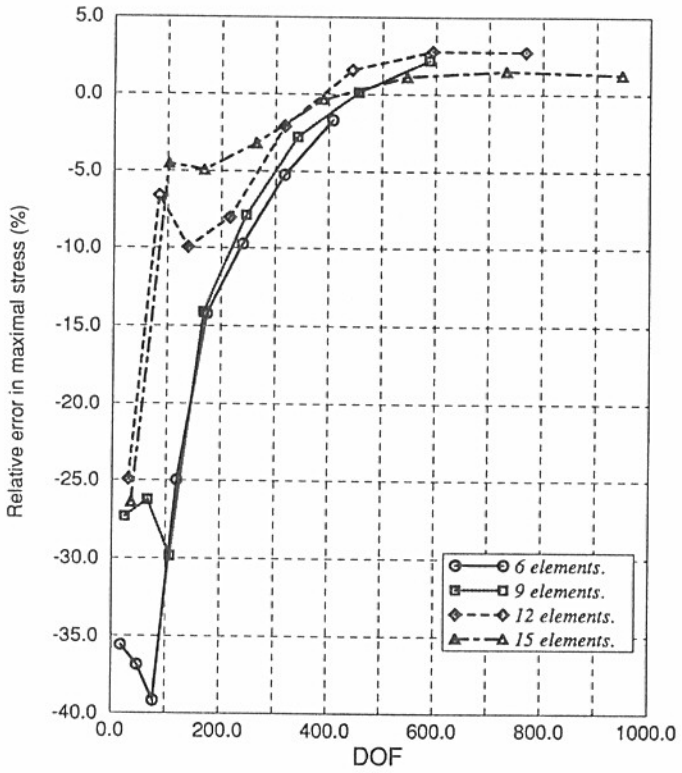

Figure 7. Convergence curves for $m = 0{\cdot}75$, regular mesh, trunk space

accurate when the product space is used, while for other cases the stress is more accurate when the trunk space is used.

Comparison between p-extensions and h-extensions

The question whether p-extensions over a fixed mesh, or h-refinement keeping $p = 2$ (constant), is better when point-wise stresses are of interest was investigated also. For this study we used the two solution domains where $m = 0{\cdot}25$ and $m = 0{\cdot}75$. The meshes used for the h-refinement study (for $m = 0{\cdot}25$) are shown in Figure 8. For the p-extensions the 6-element mesh shown in Figure 2 was used. Both the trunk and the product spaces were tested.

The error in stresses at point A is plotted against number of degrees of freedom in Figures 9 and 10 for $m = 0{\cdot}25$ and $m = 0{\cdot}75$, respectively.

It is seen that p-extension is superior to h-refinement for both cases ($m = 0{\cdot}25$ and $m = 0{\cdot}75$). For h-refinement when $m = 0{\cdot}25$, the trunk space is more efficient than the product space, while for $m = 0{\cdot}75$, the opposite is true.

Remark on cases where the stress gradients are very high

As $m \to 1$ the stress gradient increases very rapidly and the maximum stress converges progressively slower. For these cases the direct method is impractical. The following method for an indirect computation of the maximum stress is preferable.

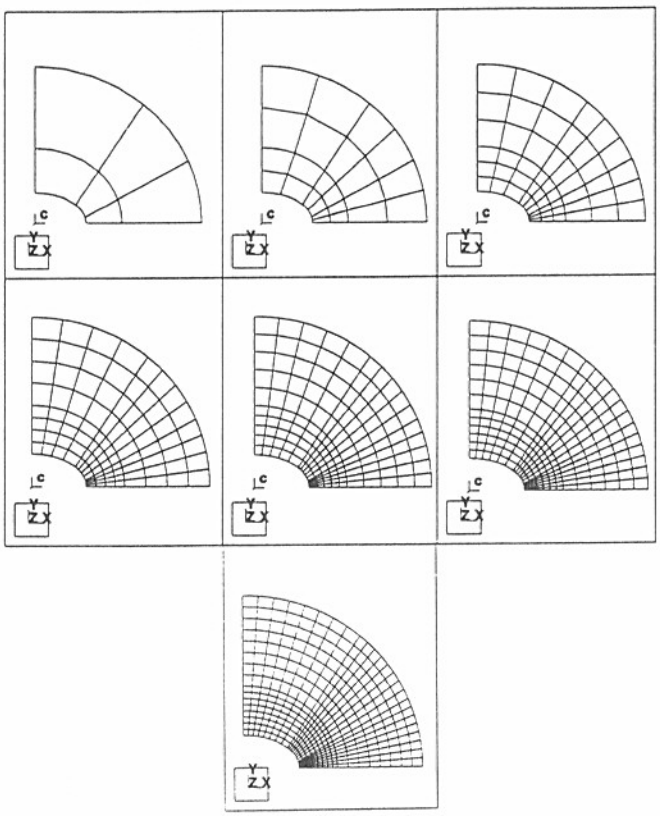

Figure 8. Sequence of h-refinements for the case $m = 0{\cdot}25$

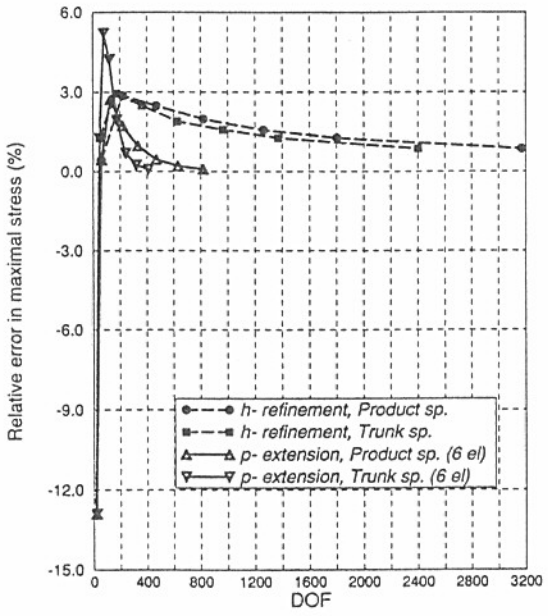

Figure 9. p- and h-convergence curves for $m = 0{\cdot}25$

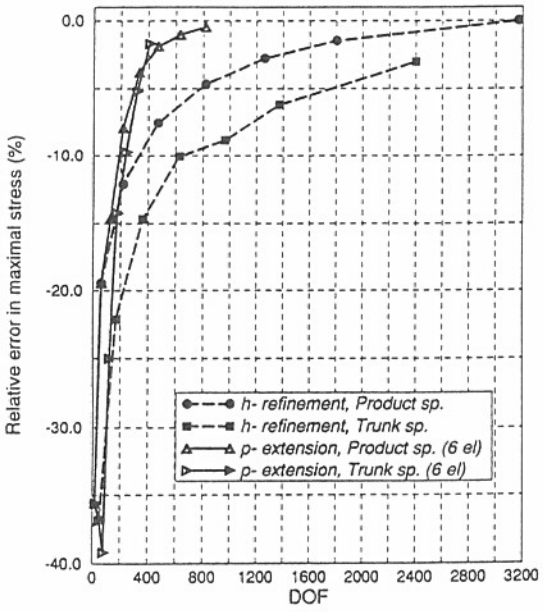

Figure 10. p- and h-convergence curves for $m = 0{\cdot}75$

A simplified solution domain, which contains a crack instead of an ellipse, is analysed. The 'stress intensity factors' for this crack tip dominate the behaviour of the stresses around it, and can be computed very accurately using superconvergent techniques (see Reference 8 for details). The local state of stress around the crack tip is dominated by the stress intensity factor, and a relationship between them for various m values can be obtained once and for all. The stress values are then obtained as a function of stress intensity factors. This approach has been tested satisfactory by Andersson *et al.*[9] and by the authors.

SUMMARY AND CONCLUSIONS

A benchmark problem was developed for testing the convergence characteristics of stress maxima in two-dimensional elasticity problems as a function of the smoothness of the exact solution. This benchmark problem was used for comparing the performance of p- and h-extensions and for investigating the question of whether a pattern exists which could be exploited for extrapolating from low-accuracy data to high-accuracy data. A large number of cases were investigated. This paper contains only a representative sample of the results. Based on this investigation, the following observations can be made:

1. There is a frequently occurring phenomenon in uniform p-extensions – the maximum stress converges from below at low p-values, 'overshoots' the exact stress value and then converges from above for higher p-values. When this pattern is visible then the error corresponding to the highest p-level is generally small (less than 3 per cent).
2. There does not appear to be a generally valid error estimation for stress maxima computed from finite element solutions. The error in energy norm can serve as a rough estimate when the solution is smooth. Generally, plots of convergence curves, similar to

those shown in Figure 3, should be used. In general, the most reliable approximation of the exact stress is the stress computed for the highest p-level.

3. The relative performance of the product and the trunk spaces with respect to increasing degrees of freedom is mixed. There does not appear to be a clear-cut advantage of one family of spaces over the other. Nevertheless, the product space yields better results for the same p-value. For this reason use of the product space in critical regions is recommended.
4. It is well known that for smooth problems p-extensions converge exponentially, whereas h-extensions converge algebraically in the energy norm. The much faster convergence of stress maxima in the case of p-extensions is evident from the results presented here.

ACKNOWLEDGEMENTS

The support of this work by the Air Force Office of Scientific Research under grant no. 92-J-0043 is gratefully acknowledged.

REFERENCES

1. I. Babuška and A. Miller, 'The post processing approach in the finite element method – part 1: Calculation of displacements, stresses and other higher derivatives of the displacements', *Int. j. numer. methods eng.*, **20**, 1085–1109 (1984).
2. K. Izadpanah, 'Computation of stress components in the p-version of the finite element method', D.Sc. dissertation, Washington University, 1984.
3. D. Vasilopoulos, 'Extraction of two-dimensional stresses on the boundary', GMR Research Publication GMR-7459, 23 August 1991.
4. N. I. Muskhelishvili, *Some basic problems of the mathematical theory of elasticity*, P. Noordhoff (Ed.), 1953.
5. C. E. Inglis, 'Stresses in a plate due to the presence of cracks and sharp corners', *Trans. Inst. Naval Architects*, London, Vol. LV, 1913, pp. 219–230.
6. I. Babuška, 'The p- and hp-versions of the finite element method: The state of the art', in D. L. Dwoyer, M. Y. Hussaini and R. G. Voigt (Eds), *Finite Elements: Theory and Application*, Springer-Verlag, 1988, pp. 199–239.
7. B. A. Szabó and I. Babuška, *Finite Element Analysis*, Wiley, 1991.
8. B. A. Szabó and I. Babuška, 'Computation of the amplitude of stress singular terms for cracks and reentrant corners', Fracture Mechanics: Nineteenth Symposium, ASTM STP 969, T. A. Cruse (Ed.), ASTM. Philadelphia, 1988, pp. 101–124.
9. B. Andersson, I. Babuška, T. von Petersdorff and U. Falk, 'Reliable stress and fracture mechanics analysis of complex aircraft components using a h-p version of FEM', The Aeronautical Research Institute of Sweden, Report no. FFA TN 1992-17, August 1992, Sweden.